Dalton Transactions

ROYAL SOCIETY OF CHEMISTRY

COMMUNICATION

View Article Online
View Journal | View Issue

Cite this: *Dalton Trans.*, 2026, **55**, 96

Received 25th August 2025,
Accepted 7th December 2025

DOI: 10.1039/d5dt02040a

rsc.li/dalton

Dinuclear *p*-cymene ruthenium hydrido complexes as active catalysts for the hydrogenation of levulinic acid to γ-valerolactone with formic acid as the hydrogen source

Boon Ying Tay, *[a] Cun Wang, [a] Davin Tan, [a] Shashikant U. Dighe, [a] Ludger Paul Stubbs, [a] Sandeep Suryabhan Gholap [a] and Han Vinh Huynh *[b]

The utilisation of mono- and bidentate *p*-cymene Ru^{II}–NHC complexes as pre-catalysts, along with formic acid as the hydrogen source, facilitates the formation of active diruthenium intermediates featuring bridging chlorido and/or hydrido ligands, which play a key role in the conversion of levulinic acid to γ-valerolactone.

As the world faces increasing challenges of fossil fuel depletion and escalating carbon dioxide emissions, there is an urgent need to explore more sustainable and environmentally benign alternatives for energy and chemical production.[1–3] Biomass stands out as a viable option, representing the sole key renewable organic carbon source.[4,5] Levulinic acid (LA) stands prominently among those molecules and has been identified by the National Renewable Energy Laboratory as one of the top twelve building block chemicals that can be produced *via* biological or chemical conversion from plant biomass.[6] γ-Valerolactone (GVL), recognised for its potential as a fuel and green solvent, can be derived from LA through catalytic hydrogenation using hydrogen gas[7] or formic acid (FA) (Fig. 1A).

Using FA as the hydrogen source offers significant advantages, particularly since FA is a co-product obtained from the typical LA production process through acid-catalysed hydrolysis.[8] Hence, it would be a resource-efficient approach as FA is already present in the reaction mixture. Furthermore, employing FA as the hydrogen source, under suitable dehydrogenation conditions, has been demonstrated to be both economically and environmentally advantageous.[9] This catalytic transformation of LA to GVL using FA represents a promising avenue for harnessing the potential of LA as a renewable platform molecule, contributing to the quest for sustainable chemical solutions.

Despite numerous studies on the homogeneous catalytic hydrogenation[10–14] of LA to GVL, few have used FA as the hydrogen source,[15,16] and there has been limited exploration into the mechanistic aspects of this process.[17,18] In 2014, Fábos *et al.* proposed the formation of a mononuclear ruthenium complex as the main catalytically active species upon dissociation of a hydrido-bridged dinuclear Shvo catalyst (Fig. 1B).[18]

In the last decade, the use of N-heterocyclic carbene (NHC) ruthenium complexes as catalysts has attracted increasing research attention.[19,20] NHCs are valued for their strong σ-donating capabilities, leading to the formation of relatively stable metal–carbon bonds.[21] Additionally, they offer excellent steric and electronic versatility,[22–26] making them attractive candidates for catalytic applications. Although Ru–NHC com-

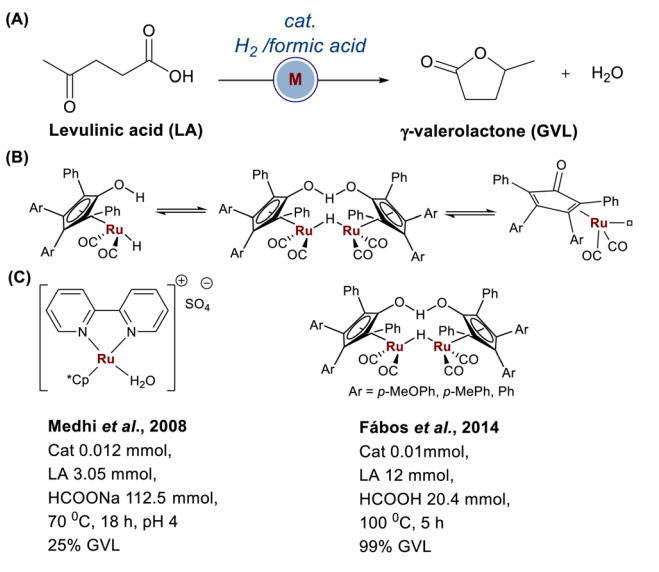

Fig. 1 (A) Conversion of LA to GVL using molecular hydrogen or formic acid as the hydrogen source, (B) Shvo's catalyst dissociation to active mononuclear species, (C) previously reported catalyst for the LA to GVL conversion using FA as the H_2 source.

[a]*Institute of Sustainability for Chemical, Energy and Environment (ISCE^2), Agency of Science, Technology and Research (A*STAR), 1 Pesek Road, Jurong Island, Singapore 627833, Republic of Singapore. E-mail: tay_boon_ying@a-star.edu.sg*
[b]*Department of Chemistry, Faculty of Science, National University of Singapore, 3 Science Drive 3, Singapore 117543, Republic of Singapore. E-mail: chmhhv@nus.edu.sg*

plexes have been extensively studied as catalysts for the hydrogenation[27,28] and transfer hydrogenation[29] of carbonyl compounds, their use in the hydrogenation of LA using FA as the hydrogen source (Fig. 1C) is relatively unexplored.[15,18,30] Hence, the design, synthesis, and mechanistic understanding of Ru–NHC catalysts for LA hydrogenation can advance the development of a more sustainable process.

In this study, seven *p*-cymene Ru(II)–NHC complexes were prepared (Fig. 2) according to a reported procedure[30] and used as the pre-catalyst in the hydrogenation of LA to GVL in the presence of FA as the hydrogen source. Complex **1a** is a new complex, and its characterisation data is provided in the SI.

The hydrogenation reactions were carried out neat at 130 °C in a closed vessel, with one molar equivalent of FA as the hydrogen source and 3 mol% NaOH. Initially, the decomposition of FA to H_2 and CO_2 led to a pressure build-up to 100 bar within the first hour, which gradually decreased thereafter (see SI for GC analysis of the gases produced). No formation of other products but GVL was detected. The summarised results are presented in Table 1.

Compared to other well-known ruthenium precursors (entries 1–4), the monocarbene complexes **1** and **2** afforded higher GVL yields (entries 5 and 7). Adding Cl substituent at 4,5-position to the imidazole (**1a**) resulted in a substantial decrease of GVL yield from 88% to 74%. Changing the NHC backbone from imidazole (**1**) to benzimidazole (**2**) led to slight improvement of the GVL yield. However, substituting the R group from an isopropyl to a benzyl group resulted in a significant decrease in GVL yield, from 91% to 72%.

Next, complexes **4–6** (entries 9–11) containing bidentate ligands were tested, and it was observed that complex **5** afforded the highest GVL yield of 83%. According to the chelate effect, as the chain length between two donor atoms increases, the chelate effect decreases.[31] This is evident in 5- and 6-membered metallacycles and becomes marginal for 7-membered metallacycle. Consequently, the 7-membered metallacycle complex **5** exhibited a higher activity compared to **4**. The weakening of the metal–carbon bond could have

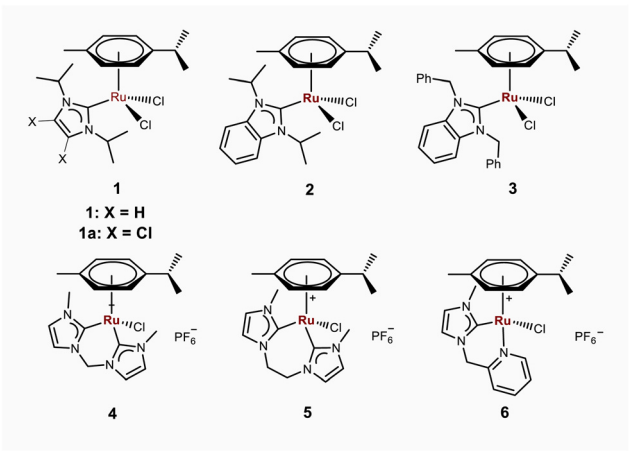

Fig. 2 Ru(II) NHC complexes **1–6** used in this study.

Table 1 Hydrogenations with FA as hydrogen source[a]

Entry	Pre-catalyst	GVL[b] (%)	TON	TOF (h^{-1})
1	Ru/C (5%)	72	953	79
2	$[RuCl_2(PPh_3)_3]$	69	920	77
3	$[RuCl_2(p\text{-cymene})]_2$	78	1044	87
4	$[RuCl_2(Cp^*)]_2$	78	1032	86
5	**1**	88	1175	98
6	**1a**	74	986	82
7	**2**	91	1209	101
8	**3**	72	964	80
9	**4**	75	997	83
10	**5**	83	1108	92
11	**6**	67	896	75

[a] Reaction condition: LA: 80 mmol, FA: 80 mmol, [Ru]: 0.075 mol%, NaOH: 2.4 mmol, 130 °C, 12 h. [b] Average of 2 runs, analysed by HPLC.

increased the lability of the ligand and enabled a vacant site for metal coordination with LA to form GVL. Complexes **4** and **6**, both 6-membered metallacycles, gave moderate GVL yields of 75% and 67% respectively. After the reaction, a homogeneous solution was obtained in all cases, and no nanoparticles were detected during TEM analysis. This is surprisingly different to when hydrogen gas was used instead of FA as the hydrogen source, which had previously resulted in the formation of Ru nanoparticles as the hydrogen atmosphere is a highly reducing environment.[30] FA, which is used as the hydrogen source in this study, needs to be decomposed into hydrogen first to create a reducing environment (which is milder than the strongly reducing hydrogen environment) to reduce LA to GVL. Besides, FA can also act as a ligand and coordinate onto the metal center.

To further elucidate and understand the role of FA in this reaction, additional experiments were carried out using complex **1** as it could be prepared in higher yields (85–90%) compared to the other complexes (15–60%). The summary of the additional experiments can be found in the SI.

First, the gases (CO_2 and H_2) generated from the decomposition of FA were released and the reactor was subsequently charged with 36 bar of hydrogen. The reaction was then allowed to proceed for an additional 11 hours, since the decomposition of FA typically requires about one hour for completion. At the end of the reaction, nanoparticles were not observed during TEM analysis and about 72% yield of GVL was obtained.

In the second experiment, carbon dioxide and hydrogen gas were charged directly into the reaction system in a 1 : 1 ratio, and the reaction was allowed to proceed. After 11 hours, Ru nanoparticles were detected (see SI) with a GVL yield of 53%. Therefore, Ru nanoparticles were formed[30] when hydrogen gas was used instead of FA as the hydrogen source, which corroborates with previous reports.[30] Additionally, a mercury-poisoning test[32] was also carried out with **1**, which revealed no evident suppression of activity. With or without mercury, the GVL yield remained the same at 79%. This result suggests that the hydrogenation occurred *via* a homogeneous pathway and not a heterogeneous one. UV analysis of the reaction mixture

with **1** and FA over a 24-hour period (six reactions were carried out at 3, 6, 9, 12, 18, 24 h) revealed the formation of a new intermediate, which remained stable throughout the process (see SI). Furthermore, ESI MS analysis of an aliquot from the reaction mixture at 30 min showed the possible presence of a dinuclear formato-bridged *p*-cymene ruthenium complex **A** (m/z = 622) without the NHC ligand (see SI). Three other dinuclear ruthenium complex fragments **B** (m/z = 578), **C** (m/z = 552) and **D** (m/z = 507) were also observed. Similar dinuclear species had been reported in the decomposition of FA catalysed by ruthenium complexes.[33,34]

Understanding reaction intermediates is crucial as they provide valuable insights into the reaction mechanism. To this end, we endeavoured to isolate and elucidate the structures of these intermediates. Complex **1** was mixed with 130 equiv. of FA and heated at 60 °C for 3 hours. Subsequent TLC separation of the crude products gave two fractions. One fraction contained pure product **7**, which is a hydrido- and chlorido-bridged diruthenium complex (Fig. 3) and was characterised by ^{1}H NMR analysis. The other was a mixture of **7** and **8**, whereby **8** is a diruthenium complex with an additional formato-bridge. In the ^{1}H NMR spectrum of **7**, the bridging hydrido exhibits a characteristic chemical shift at −10.17 ppm, similar to the previously reported value of −10.10 ppm.[35] Complex **8** is labile and tends to convert to complex **7** by losing one molecule of carbon dioxide in an acidic environment (silica gel is acidic and contains residual chloride). This explains our initial observation of a mixture of **7** and **8** during the first TLC separation. While we were unable to isolate pure **8**, ^{1}H NMR analysis of the mixture of **7** and **8** showed the typical chemical shifts for the hydrido (−6.97 ppm) and formato-bridges (6.81 ppm) with integrals in a 1 : 1 ratio (see SI). These chemical shifts are consistent with those reported previously.[17] To confirm that other pre-catalysts also form **7** and **8**, we used complex **2** under identical experimental conditions, and ^{1}H NMR analysis revealed the same chemical shifts we observed previously.

We also attempted to react $[RuCl_2(p\text{-cymene})]_2$ with 130 equiv. of FA at 60 °C for 3 hours to prepare **7** but recovered the complex unchanged upon the removal of FA. Since it has been shown that $[RuCl_2(p\text{-cymene})]_2$ yields **7** in the presence of triethylamine under 4 atm of hydrogen,[35] we presume that the basic NHC ligand facilitates the formation of **7**.

Attempts to grow and obtain diffraction-quality crystals of **7** were unsuccessful. Nevertheless, we were able to synthesize and isolate the more stable *p*-cymene μ-hydrido/μ-bromido diruthenium complex **9** (an analogue of **7**), confirming its structure through NMR, MS, EA, and single-crystal XRD analysis (Fig. 4, SI), achieved by a halogen exchange from Cl to Br. This μ-hydrido-bridged dinuclear ruthenium complex was then used directly in the hydrogenation of LA to GVL under the same conditions and yielded similarly good results (88% yield). The exchange of chlorido ligand to bromido ligand is expected to have a minor effect on the catalytic activity in transfer hydrogenations.[36] Our findings suggest that FA undergoes catalytic decomposition to produce hydrogen gas and carbon dioxide, leading to the formation of the stable dinuclear ruthenium complex. In this case, FA serves as both the hydrogen source for the transfer hydrogenation process and as a facilitator in the formation of diruthenium active species that catalyses the transformation of LA to GVL.

To investigate whether the presence of an organic acid can stabilise the dinuclear ruthenium species instead of reduction to Ru nanoparticles, we added one equivalent of acetic acid to the reaction mixture charged with 36 bar of hydrogen gas and complex **1** for 11 hours. At the end of the reaction, ruthenium plating was formed on the reaction liner, with 28% GVL formed, and nanoparticles were detected during TEM analysis (see SI). Under such a reducing hydrogen atmosphere, **7** can be rapidly converted to ruthenium nanoparticles.[37,38] In the absence of hydrogen gas, the soluble ruthenium complex remains in the reaction mixture. Upon heating **9** with excess acetic acid at 130 °C, and after TLC separation using DCM : MeOH in a 9 : 1 ratio, compound **10** (Fig. 3) was isolated and characterised by ^{1}H and ^{13}C NMR (see SI). We also conducted an experiment using 2-butanone as a simple aliphatic 2-oxoalkane under identical reaction conditions. The 2-butanol yield was quantified by ^{1}H NMR to be 65%, suggesting that the ketone group in 2-butanone is hydrogenated more slowly than the ketone group in LA. It is believed that the carboxyl group of the LA is important as it needs to anchor onto the diruthenium complex for hydrogenation of LA to proceed. With supported metal catalysts,[39] the hydrogenation of LA and 2-pentanone, showed similar reaction rates under comparable conditions.

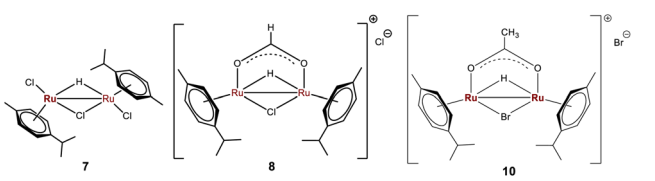

Fig. 3 Schematic representation of **7**, **8** and **10**.

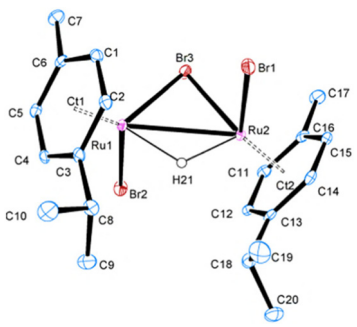

Fig. 4 Molecular structure of **9** with thermal ellipsoids drawn at 30% probability level. Hydrogen atoms and solvent molecules are omitted for clarity. Selected bond lengths (Å) and bond angles (°): Ru(1)–Ru(2) 2.9928(7), Br(1)–Ru(2) 2.5528(7), Br(2)–Ru(1) 2.5320(6); Br(3)–Ru(2)–Br(1) 90.91(2), Br(2)–Ru(1)–Br(3) 89.77(2).

Based on all these results, we propose the following mechanism. The dinuclear ruthenium complex **8** first forms from the carbene complex **1** (Fig. 5) in the presence of FA. The ease of forming **8** depends on the ease of dissociation of the carbene ligands when protonolysis of the Ru–NHC happens in the presence of FA. Although it has been well-known that M–σ bonds are quite strong, M–NHC bonds can be cleaved *via* reductive elimination, protonolysis and ligand displacement.[40] Protonation of M–NHC complexes with Brønsted acid results in the loss of the imidazolium salt.[41,42] During this process, the carbene ligand dissociates from the Ru center, releasing hydrogen chloride as a by-product. The free NHC ligand (m/z = 153) was detected and observed as an imidazolium cation in ESI-MS (see SI.) Sodium hydroxide was added as a base to promote this reaction. Complex **8** then enters the first catalytic cycle I, whereby FA decomposes into hydrogen gas and carbon dioxide, which forms **7**, the resting state. Analogous dinuclear Ru–H species have similarly been identified as resting states in related catalytic systems.[43] In cycle II, LA reacts with **7** to form intermediate **11**, which we suggest to be the rate-determining step. Subsequently, the hydride attacks the carbonyl group of the LA to form the hemi-acetal cyclic lactone, denoted as intermediate **12**. Upon addition of hydrogen, which was formed from cycle I, the resulting intermediate **13** regenerates back to **7**, releasing GVL and a molecule of water. Consequently, with the addition of another molecule of FA, **7** restores back to **8**, completing both catalytic cycles. Alternatively, intermediate **13** could directly react with LA to intermediate **11**, forming a separate catalytic cycle independent of the FA decomposition. Further kinetic and computational modelling studies could elucidate the mechanism. Unlike cycle I where carbon dioxide formed as the by-product, in cycle II, GVL and water are released as the main products. To prove the formation of intermediate **11**, compound **9** (Br analogue of **7**) was heated to 130 °C with 5 equivalents of LA in MeOH. Upon TLC separation with DCM : MeOH in a 9 : 1 ratio, the bromido-equivalent of **11** was successfully obtained and was characterised by ^{1}H NMR (see SI), justifying the proposed catalytic mechanism. Noteworthily this mechanism differs significantly from previous work[19] where the dissociation of the dinuclear Shvo's catalyst formed a mononuclear ruthenium complex, which was proposed to be the main catalytically active species. Whilst here, the unexpected dissociation of the NHC ligand led to the experimentally observed diruthenium complexes **7** and **8** that are believed to be the key active species in both catalytic cycles I and II. We were unable to detect the transient intermediates corresponding to complexes **12** and **13** by NMR or ESI-MS as they are short-lived and are rapidly consumed in the subsequent reaction step, making their direct observation challenging under the current experimental conditions.

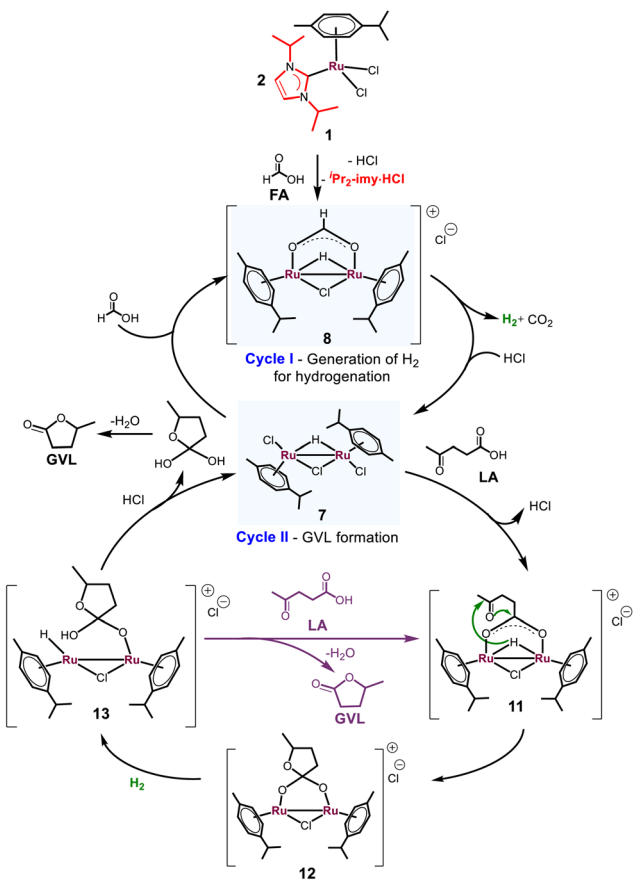

Fig. 5 Proposed mechanism for the formation of dinuclear ruthenium complexes and the catalytic cycles to reduce LA to GVL.

Conclusions

In conclusion, we have successfully synthesized and evaluated seven *p*-cymene Ru(II)–NHC complexes as pre-catalysts for the hydrogenation of levulinic acid (LA) to γ-valerolactone (GVL), using formic acid (FA) as the hydrogen donor. FA was found to promote the formation of a formato-bridged, and subsequently a hydrido-bridged, dinuclear ruthenium complex. This dinuclear species was successfully isolated, fully characterised and is proposed to be the true active catalytic intermediate in the reaction. Interestingly, the labile NHC ligand appears to play only a peripheral role—facilitating the formation of the dinuclear *p*-cymene ruthenium complexes—without participating directly in the catalytic cycle. This unexpected behaviour challenges previous assumptions about the robustness and coordination strength of NHC ligands under reducing conditions. We hope these findings provide new insights into the mechanistic complexity of this catalytic transformation and contribute to the rational design of more efficient molecular catalysts for biomass valorisation.

Author contributions

B. Y. Tay: conceptualisation, methodology, investigation, validation, writing original draft. C. Wang: formal analysis, discussion, writing, review, and editing. D. Tan: writing, discussion, review, and editing. S. U. Dighe: visualisation, writing, review,

and editing. L. P. Stubbs: discussion, writing, review, and editing, supervision. S. S. Gholap: discussion, writing, review, and editing. H. V. Huynh: supervision, discussion, writing, review, and editing.

Conflicts of interest

There are no conflicts to declare.

Data availability

The data supporting this article have been included as part of the supplementary information (SI). Supplementary information: experimental details; selected crystallographic data; NMR spectra; MS spectra; TEM image; UV spectra; GC, HPLC chromatograms and crystallographic data. See DOI: https://doi.org/10.1039/d5dt02040a.

CCDC 2336954 (**9**) contains the supplementary crystallographic data for this paper.[44]

Acknowledgements

We thank the Singapore Science and Engineering Research Council (SERC Grant 0921590134), A*STAR HTCO Seed Fund (C231218003) and A*STAR RIE2025-IEO Decentralised GAP Fund (I24D1AG008) for funding support, Ms Angeline Seo for her assistance in elemental analysis and Ms Chia Sze Chen for her assistance with X-ray crystallographic analysis.

References

1 L. Yan, Q. Yao and Y. Fu, *Green Chem.*, 2017, **19**, 5527–5547.
2 M. J. Climent, A. Corma and S. Iborra, *Green Chem.*, 2014, **16**, 516–547.
3 Global Monitoring Laboratory – Carbon Cycle Greenhouse Gases, https://gml.noaa.gov/ccgg/trends/global.html, (accessed 13 February 2024).
4 G. W. Huber, S. Iborra and A. Corma, *Chem. Rev.*, 2006, **106**, 4044–4098.
5 A. Corma, S. Iborra and A. Velty, *Chem. Rev.*, 2007, **107**, 2411–2502.
6 T. Werpy and G. Peterson, *U.S. Department of Energy NREL/TP-510-35523,* 2004, pp. 45–48.
7 K. Zhang, J. Wang, Y. Tian, S. Zhang, S. S. Chen, L. Cao, J. Zhang, J. H. Clark and S. Zhang, *iScience*, 2025, **28**, 112734–112786.
8 D. W. Rackemann and W. O. S. Doherty, *Biofuels, Bioprod. Biorefin.*, 2011, **2**, 198–214.
9 A. Wang, P. He, J. Wu, N. Chen, C. Pan, E. Shi, H. Jia, T. Hu, K. He, Q. Cai and R. Shen, *Energy Fuels*, 2023, **37**, 17075–17093.
10 K. Osakada, T. Ikariya and S. Yoshikawa, *J. Organomet. Chem.*, 1982, **231**, 79–90.
11 J. M. Tukacs, D. Király, A. Strádi, G. Novodarszki, Z. Eke, G. Dibó, T. Kégl and L. T. Mika, *Green Chem.*, 2012, **14**, 2057–2065.
12 F. M. A. Geilen, B. Engendahl, A. Harwardt, W. Marquardt, J. Klankermayer and W. Leitner, *Angew. Chem., Int. Ed.*, 2010, **49**, 5510–5514.
13 W. Li, J.-H. Xie, H. Lin and Q.-L. Zhou, *Green Chem.*, 2012, **9**, 2388–2390.
14 M. Chalid, A. A. Broekhuis and H. J. Heeres, *J. Mol. Catal. A: Chem.*, 2011, **341**, 14–21.
15 H. Mehdi, V. Fábos, R. Tuba, A. Bodor, L. T. Mika and I. T. Horváth, *Top. Catal.*, 2008, **48**, 49–54.
16 L. Deng, J. Li, D.-M. Lai, Y. Fu and Q.-X. Guo, *Angew. Chem., Int. Ed.*, 2009, **48**, 6529–6532.
17 M. Czaun, A. Goeppert, R. May, R. Haiges, G. K. S. Prakash and G. A. Olah, *ChemSusChem*, 2011, **4**, 1241–1248.
18 V. Fábos, L. T. Mika and I. T. Horváth, *Organometallics*, 2014, **33**, 181–187.
19 X. Xie and H. V. Huynh, *ACS Catal.*, 2015, **5**, 4143–4151.
20 A. M. Seayad, S. P. Shan, X. Xiaoke, B. Gnanaprakasam, T. T. Dang, B. Ramalingam and H. V. Huynh, *RSC Adv.*, 2015, **5**, 4434–4442.
21 H. V. Huynh, *The Organometallic Chemistry of N-heterocyclic Carbenes*, John Wiley & Sons Ltd, UK, 2017.
22 H. V. Huynh, *Chem. Rev.*, 2018, **118**, 9457–9492.
23 F. E. Hahn and M. C. Jahake, *Angew. Chem., Int. Ed.*, 2008, **47**, 3122–3172.
24 S. Kuwata and F. E. Hahn, *Chem. Rev.*, 2018, **118**, 9642–9677.
25 L. Cavallo, A. Correa, C. Costabile and H. Jacobsen, *J. Organomet. Chem.*, 2005, **690**, 5407–5413.
26 L. Benhamou, E. Chardon, G. Lavigne, S. Bellemin-Laponnaz and V. César, *Chem. Rev.*, 2011, **111**, 2705–2733.
27 W. N. O. Wylie, A. J. Lough and R. H. Morris, *Organometallics*, 2012, **31**, 2137–2151.
28 F. A. Westerhaus, B. Wendt, A. Dumrath, G. Wienhöfer, K. Junge and M. Beller, *ChemSusChem*, 2013, **6**, 1001–1005.
29 X.-W. Li, G.-F. Wang, F. Chen, Y.-Z. Li, X.-T. Chen and Z.-L. Xue, *Inorg. Chim. Acta*, 2011, **378**, 280–287.
30 B. Y. Tay, C. Wang, P. H. Phua, L. P. Stubbs and H. V. Huynh, *Dalton Trans.*, 2016, **45**, 3558–3563.
31 K. L. Haas and K. J. Franz, *Chem. Rev.*, 2009, **109**, 4921–4960.
32 J. E. Hamlin, K. Hirai, A. Millan and P. M. Maitlis, *J. Mol. Catal.*, 1982, **15**, 337–347.
33 D. J. Morris, G. J. Clarkson and M. Wills, *Organometallics*, 2009, **28**, 4133–4140.
34 J. D. Scholten, M. H. G. Prechtl and J. Dupont, *ChemCatChem*, 2010, **2**, 1265–1270.
35 M. A. Bennett and J. P. Ennett, *Organometallics*, 1984, **3**, 1365–1374.
36 P. Weingart, Y. Sun and W. R. Thiel, *ChemCatChem*, 2020, **12**, 6223–6233.
37 Y. Lin and R. G. Finke, *Inorg. Chem.*, 1994, **33**, 4891–4910.

38 J. A. Widegren, M. A. Bennett and R. G. Finke, *J. Am. Chem. Soc.*, 2003, **125**, 10301–10310.
39 O. A. Abdelrahman, H. Y. Luo, A. Heyden, Y. Román-Leshkov and J. Q. Bond, *J. Catal.*, 2015, **329**, 10–21.
40 V. M. Chernyshev, E. A. Denisova, D. B. Eremin and V. P. Ananikov, *Chem. Sci.*, 2020, **11**, 6957–6977.
41 O. Saker, M. F. Mahon, J. E. Warren and M. K. Whittlesey, *Organometallics*, 2009, **28**, 1976–1979.
42 M. Rouen, P. Queval, L. Falivene, J. Allard, L. Toupet, C. Crévisy, F. Caijo, O. Baslé, L. Cavallo and M. Mauduit, *Chem. – Eur. J.*, 2014, **20**, 13716–13721.
43 C. P. Casey, S. E. Beetner and J. B. Johnson, *J. Am. Chem. Soc.*, 2008, **130**, 2285–2295.
44 CCDC 2336954: Experimental Crystal Structure Determination, 2025, DOI: 10.5517/ccdc.csd.cc2jfsmd..